Interface Stabilization in Adhesion Caused by Elastohydrodynamic Deformation

Preetika Karnal,[1,2] Yumo Wang,[3] Anushka Jha,[1] Stefan Gryska,[4] Carlos Barrios,[5] and Joelle Frechette[6,*]
[1]Department of Chemical and Biomolecular Engineering, Johns Hopkins University, 3400 North Charles Street, Baltimore, Maryland 21218, USA
[2]Department of Chemical and Biomolecular Engineering, Lehigh University, 124 East Morton Street, Building 205, Bethlehem, Pennsylvania 18015, USA
[3]College of Mechanical and Transportation Engineering, China University of Petroleum, Beijing 102249, China
[4]3M Center, 3M Company, Building 201-4N-01, St. Paul, Minnesota 55144-1000, USA
[5]Adaptive3D, 608 Development Drive, Plano, Texas 75074, USA
[6]Department of Chemical and Biomolecular Engineering, University of California Berkeley, Berkeley, California 94720, USA

(Received 15 January 2023; accepted 22 August 2023; published 25 September 2023)

Interfacial instabilities are common phenomena observed during adhesion measurements involving viscoelastic polymers or fluids. Typical probe-tack adhesion measurements with soft adhesives are conducted with rigid probes. However, in many settings, such as for medical applications, adhesives make and break contact from soft surfaces such as skin. Here we study how detachment from soft probes alters the debonding mechanism of a model viscoelastic polymer film. We demonstrate that detachment from a soft probe suppresses Saffman-Taylor instabilities commonly encountered in adhesion. We suggest the mechanism for interface stabilization is elastohydrodynamic deformation of the probe and propose a scaling for the onset of stabilization.

DOI: 10.1103/PhysRevLett.131.138201

There is a wide interest in controlling interfacial instabilities, as they often affect the process in which they are formed [1–11]. Interfacial instabilities can be a safety hazard for batteries [12,13], limit oil recovery [14], impact properties of graphene sheets [15], enhance the mixing of fluids [16,17], or guide the fabrication of soft materials [18–20]. A common interfacial instability is the Saffman-Taylor type, manifested as undulating patterns formed in narrow gaps at fluid-fluid interfaces when a lower viscosity fluid displaces a higher viscosity fluid [21–25]. Their onset can be controlled through low flow rates [25] or local geometry [1,2,26]. For example, elastic deformation of a membrane ahead of the fluid-fluid front alters the flow and suppresses viscous instabilities [10,27]. Because of their sensitivity to the flow profile, interfacial instabilities could potentially be manipulated in contact problems, such as in adhesion, where they are a source of energy dissipation [22,24,28–30].

Adhesion between two soft materials is ubiquitous during contact with skin with medical adhesives or flexible electronics [43–48]. Despite its technological significance, studies of adhesion between two soft materials are limited, but reveal qualitative differences from debonding from a rigid surface [49–56]. Here we show how the mode of debonding between a soft spherical probe and a thin viscoelastic adhesive film is altered as the compliance of the probe increases [Fig. 1(a)]. Saffman-Taylor instabilities are present during the detachment of a spherical rigid probe from a viscoelastic film (a variation of lifted Hele-Shaw cells). However, we find that the interface stabilizes when the compliance of the probe increases. The spherical probes studied are silicone elastomers for which we systematically vary the compliance, while the opposing surface is a soft viscoelastic pressure sensitive adhesive (PSA) film. We hypothesize that elastohydrodynamic deformation of the spherical probe, caused by the viscous forces within the adhesive film during retraction, stabilizes the interface.

As control experiments, we measured the force in air during the detachment of rigid glass probes from the viscoelastic adhesive [thickness of $b = 25$ μm, Young's modulus ~30 kPa, Fig. 1(a)]. The adhesion measurements are conducted on a microscope with bottom and side view imaging [57]. During detachment, the adhesive-air interface is unstable and fingers form and grow until complete debonding [Fig. 1(c)]. A distinguishing feature of interfacial instabilities in adhesion is the dependence of their wavelength λ on the detachment velocity. For a Saffman-Taylor instability, λ scales with the film thickness (b) and the Capillary number ($Ca = \eta^* U/\gamma$) as

$$\lambda = \pi b/\sqrt{Ca}, \tag{1}$$

where η^* is the complex viscosity of the adhesive, U is the radial velocity, and γ is the surface tension of the adhesive-air interface [23,25,27,28]. The complex viscosity accounts for the viscoelasticity of the adhesive. We measured adhesion for different detachment velocities and film thicknesses (25–100 μm) and characterized fingering wavelengths at their onset (lowest strain in the films).

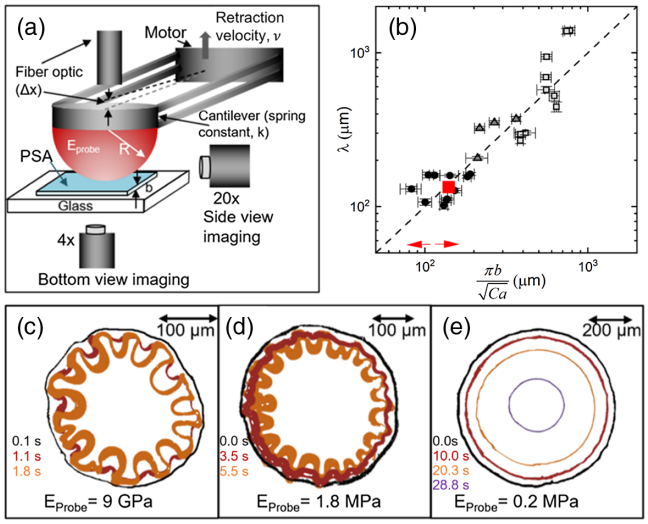

FIG. 1. (a) Schematic (not to scale) of measurements [31]. (b) Validation of Eq. (1). Data from debonding between rigid probes and adhesive films of $b = 25$ (circle), 50 (triangle), and 100 μm (square). Arrows indicate the expected range for soft probes with $b = 25$ μm. Unstable interface for $b = 50$ μm for $E_{\text{probe}} = 1.8$ MPa (red square). (c)–(e) Superimposed contours of bottom view of the adhesive-air interface at different times during retraction from probes of different moduli. Initial contact line is in black. Interface moves radially inward during retraction. Unstable interface (c),(d) shows fingering as opposed to a stable interface (e).

We then compared our measurements to Eq. (1) by determining the capillary number using the radial velocity of the growing fingers' apex, the complex viscosity η^*, and the surface tension (45 ± 2 mN/m) [31,58]. Agreement between data and Eq. (1): Fig. 1(b), confirms the presence of Saffman-Taylor instabilities (see Supplemental Material [31]). In contrast, an elastic instability in the PSA would have a wavelength that only depends on the thickness of the adhesive ($\lambda_e = 4b$) [31,59–62] and quadruples as we quadruple the film thickness. Instead, if we quadruple the thickness, the wavelength increases by a factor of 3–12 depending on the velocity, with the wavelength decreasing as the velocity increases, both characteristic of Saffman-Taylor instabilities.

We then repeat the same measurements, but with silicone probes of increasing compliance. The compliant probes are made of polydimethyl siloxane (PDMS) of different cross-linking ratios that were extracted after curing to remove unreacted oligomers and treated with plasma to render their surface hydrophilic. The soft probes have nearly identical geometry and surface energy as the rigid probes, but with a Young's modulus that varies from ~2 to ~0.2 MPa [31]. We estimate the Ca of the adhesive film during the detachment and found it comparable to values for rigid probes that displayed Saffman-Taylor instabilities [red arrows, Fig. 1(b)]. Detachment with the stiffer PDMS leads to an unstable interface, but the interface stabilizes for softer probes [Figs. 1(d) and 1(e)].

Because of confinement, the compliance of the adhesive film is smaller than its bulk counterpart and also smaller than all soft probes investigated [31]. While a PSA is a viscoelastic solid, a simple stress-strain model where the thin adhesive film is in series with a soft probe ($k_{\text{PSA}} \gg k_{\text{Probe}}$) suggests a significant dissipative response due to the complex viscosity of the adhesive [31]. Therefore, even if the adhesive film is a solid, its dynamic response is dominated by viscoelasticity. Moreover, recent work shows that in the case of elastic instabilities the interface can become stable as the probe modulus increases; the opposite of our observations [63].

As the probe compliance increases, the interface becomes stable during detachment [Figs. 1(c)–1(e)]. Because only the compliance of the probe is varied (and not its surface energy), the experiments suggest the importance of compliance on interface stabilization [31]. The transition to a stable interface also has no impact on the adhesive strength (F_{max} in Fig. 2, inset). For the same debonding velocity, the adhesive strength is nearly the same for all probe moduli, without any distinction between stable and unstable interfaces. For the sphere-plane geometry, the adhesive strength is independent of compliance, but the mode of failure can affect the force profile [64,65]. A small

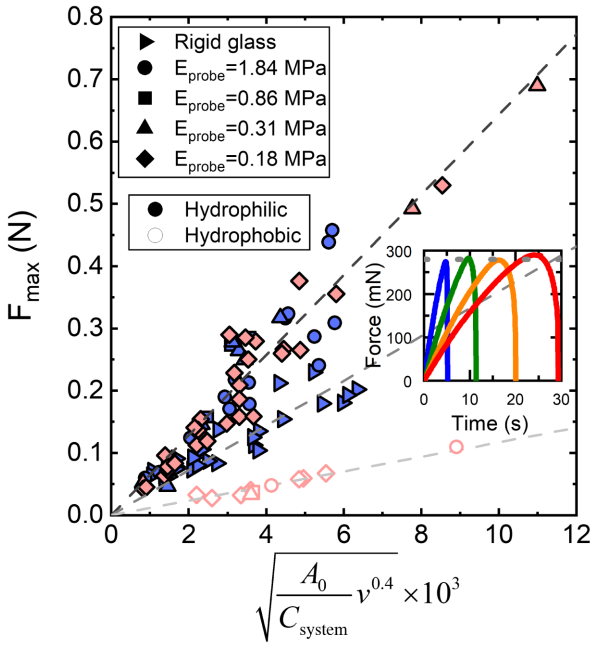

FIG. 2. Adhesive strength for different probes and retraction velocities. The slope $\sim(2\sqrt{G_0/v_{\text{ref}}^{0.4}})$ increases with probe surface energy. There is no distinction in the adhesive strength for a stable (pink) or unstable (blue) interface. Inset: debonding curve between soft PDMS probes and adhesive films at $v = 50$ μm/s. Increase in probe compliance leads decreases the slope. The maximum force F_{max} is independent of probe modulus.

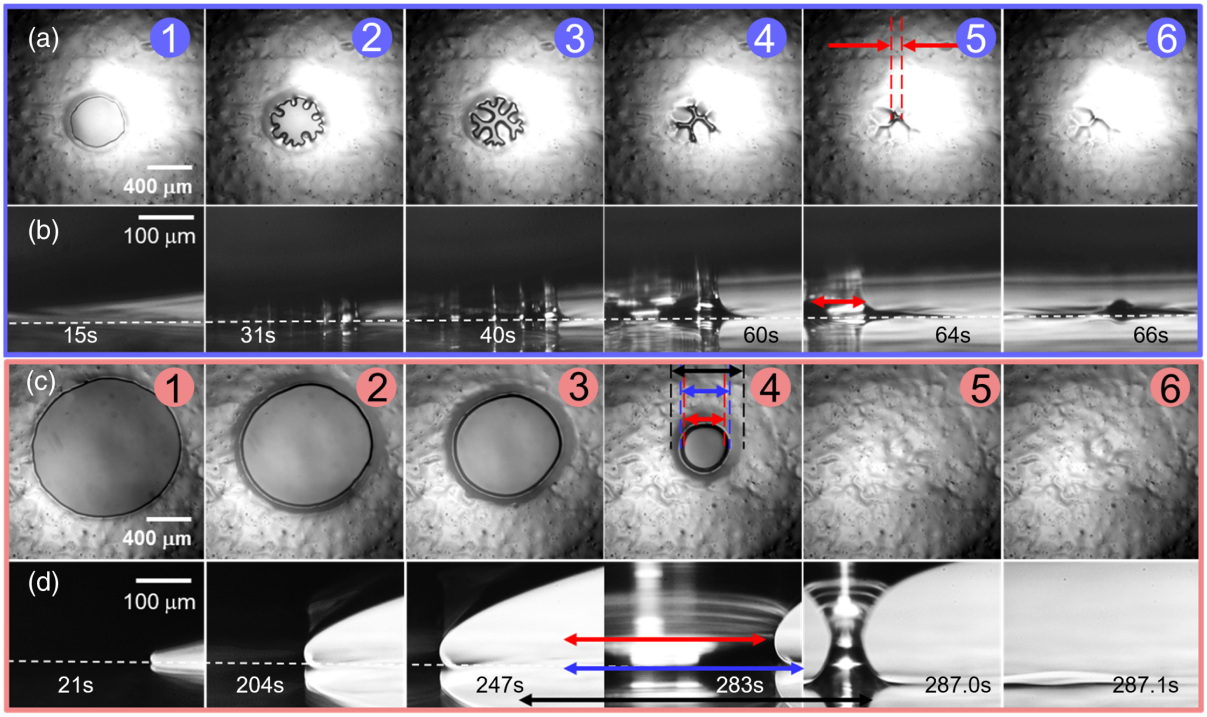

FIG. 3. Side and bottom view images during debonding over time. Rigid probe (a) bottom and (b) side views. Soft probe, $E_{\text{probe}} = 0.18$ MPa (c) bottom and (d) side views. Instabilities are present during debonding from the rigid probe. Side view images (b) show stretching of adhesive. For the soft probe (c) the interface is stable, side views (d) show probe deformation. Note the different scale and magnification between the side and bottom views; the arrows represent the same dimension.

plateau in force was also observed with the onset of fingering instabilities when lifting rigid plates confining viscous fluid [29], whereas adhesion-induced elastic instabilities increased the resistance to deformation leading to higher forces [66].

We also find that stabilization of the interface is not due to a change in probe surface energy. The relationship between the adhesive strength (F_{max}), debonding velocity (v), and compliance is well established and given by

$$F_{\text{max}} = 2\left[\frac{A_0}{C_{\text{sys}}} G_0 \left(\frac{v}{v_{\text{ref}}}\right)^n\right]^{\frac{1}{2}}, \tag{2}$$

where G_0 is the intrinsic strain energy release rate, A_0 is the maximum contact area, C_{sys} is the system compliance, v is the debonding velocity, and n is an empirical constant, here $n = 0.4$ [31,64,65,67]. Therefore, for a constant apparent work of adhesion, we expect a linear relationship between F_{max} and $\sqrt{A_0/C_{\text{sys}} v^{0.4}}$ with a slope $2\sqrt{G_0/v_{\text{ref}}^{0.4}}$. Adhesion follows well the established force scaling relationship, with no departure from the linear relationship that would indicate a change in surface energy for softer PDMS probes. Data for the hydrophilic PDMS include the adhesive strength for probes with elastic moduli between 0.18 and 1.8 MPa (Fig. 2) (see Supplemental Material [31]). The linear relationship observed across PDMS probe moduli confirms the constant apparent surface energy. This linear relationship also holds for probes of different surface energy, but with a different slope (silica and hydrophobic PDMS, Fig. 2).

Side view imaging shows that transition to a stable interface is accompanied by significant elastic deformation of the probe, Fig. 3. The forces resisting the probe's upward motion within the adhesive film cause elastic deformation of the probe and appear to be stabilizing the interface. For hydrophilic PDMS probes, interface stabilization occurs despite having the same intrinsic surface energy. Using $G_0/E_{\text{eff}}a$, we evaluate the intrinsic strain energy release rate normalized with the contact compliance (or the elastoadhesive length normalized with the contact radius) [68], where the effective modulus is $E_{\text{eff}} = 3/4C_{\text{sys}}a$, and a is the contact radius. This quantity represents the ability of a material to resist crack propagation through elasticity. Changes in the relative importance between contact compliance and surface energy in the contact region (G_0a^2), Fig. 4(a), do not delineate stable from unstable interfaces. In other words, the deformation of the probe is not dominated by an increased contribution from the surface energy as the probe modulus decreases.

Here, debonding occurs between a soft probe and a viscoelastic adhesive. At any given time, the measured force is due to surface, viscoelastic, and elastic (probe deformation) contributions. The elastic (probe deformation) and viscous ("flow" of the adhesive) forces are highly

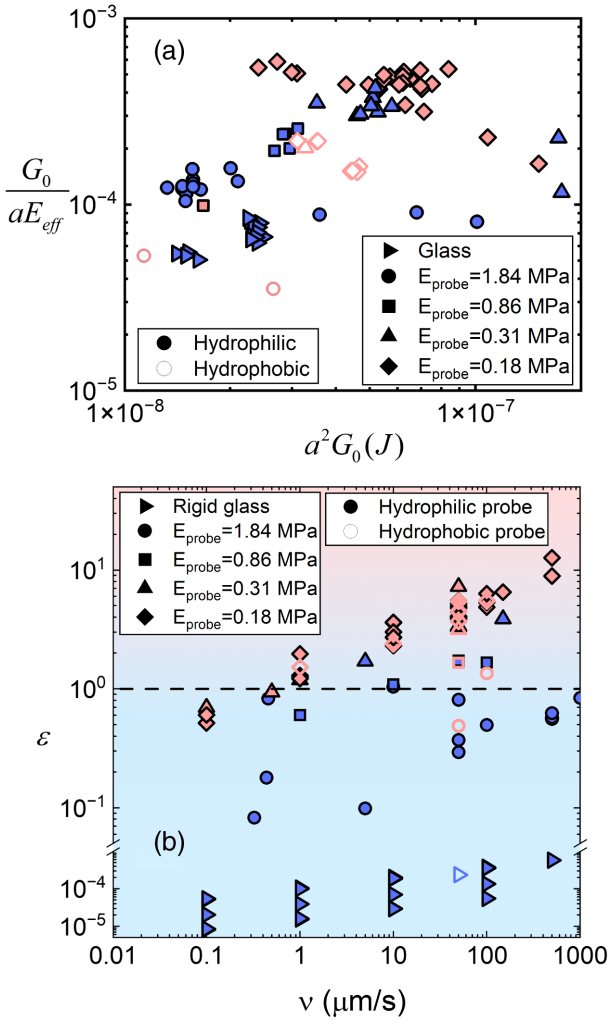

FIG. 4. (a) Elastoadhesive length normalized by the contact radius vs effective surface energy for all probes. (b) Elasticity parameter (ϵ) vs debonding velocity (v). The transition from unstable to stable interface is observed around $\epsilon = 1$ (black dotted line). Data include adhesive with $b = 25$, $b = 50$, $b = 100$ μm, and R between 4.5 and 14 mm and shows unstable interface (blue) and stable interface (pink).

coupled. Elastohydrodynamic deformation occurs when the viscous forces in a fluid are strong enough to cause elastic deformation to an opposing surfaces [69–72]. We hypothesize that the probe deformation alters the pressure distribution within the adhesive film, leading to a suppression of Saffman-Taylor instabilities. The relative importance of elastohydrodynamic deformation can be estimated through an elasticity parameter ϵ [Eq. (3)], obtained from nondimensionalization of the lubrication equation [69,70,73],

$$\epsilon = \frac{\eta^* v R^{1.5}}{E^*_{\text{probe}} b^{2.5}}. \tag{3}$$

The elasticity parameter can be viewed as a ratio between elastic forces within the probe and viscous forces within the adhesive film. As ϵ increases, the elastic deformation of the probe (w) increases. For low ϵ, viscous forces do not cause probe deformation. We previously found that the dimensionless central deformation ($\hat{w} = w/b$) of a spherical probe scales with $(6\epsilon)^{0.4}$ [74].

A plot of ϵ as a function of debonding velocity (v) shows a clear demarcation between stable and unstable interfaces [Fig. 4(b)]. The transition to a stable interface occurs across different materials systems and experimental parameters: probe modulus, radius, detachment velocity, and film thickness. The transition between an unstable and stable interface occurs around $\epsilon = 1$, when the elastic forces in the probe begin to dominate over the viscous forces in the adhesive film. The transition to a stable interface as the elasticity parameter increases supports the hypothesis that elastohydrodynamic deformation of the probes suppresses the fingering instabilities.

As the velocity increases, the adhesive strength increases, and stabilization of the interface shifts to higher ϵ [Fig. 4(b)]. We compare the role of debonding velocity on the probe deformation and the pressure within the film. An increase in v will increase the pressure within the adhesive film, which has a destabilizing tendency for the interface. However, increasing the velocity also increases the probe deformation, which we hypothesize stabilizes the interface. Nondimensionalization of the lubrication equation leads to a characteristic pressure in the fluid, $p^* = \eta v R/b^2$ [74]. For a viscoelastic film, $p^* = \eta^* v R/b^2$, therefore $p^* \propto v^{(1-m)}$ with the dependence of the complex viscosity on velocity. For our material here $m = 0.725$, giving $p^* \propto v^{0.28}$. Moreover, the dimensionless central probe deformation scales as $\hat{w} \sim v^{0.4(1-m)}$ and, specifically for our material system, $\hat{w} \sim v^{0.11}$. Therefore, as v increases, the pressure within the film ($p^* \sim v^{0.28}$) increases faster than the deformation of the probe ($\hat{w} \sim v^{0.11}$). The faster increase in pressure within the film as v increases would necessitate larger probe deformations to stabilize the interface; thus a higher elasticity parameter is needed for stabilization.

We study the relationship between elastohydrodynamic deformation and adhesive film pressure by modeling debonding between a soft probe and a rigid surface submerged in a Newtonian fluid (see Supplemental Material [31]). In the model, the fluid viscosity is comparable to the complex viscosity of the adhesive. This model is a highly simplified version of our experiments, in that the adhesive is treated as a viscous fluid without an air-adhesive interface present. We extract the pressure profile during detachment for both rigid and soft probes and obtain lower fluid pressure with the soft probe, Fig. 5, which would have a stabilizing effect. We also observe that the elastohydrodynamic probe deformation leads to a non-monotonous pressure drop within the fluid. In contrast, the pressure distribution is monotonic during the detachment

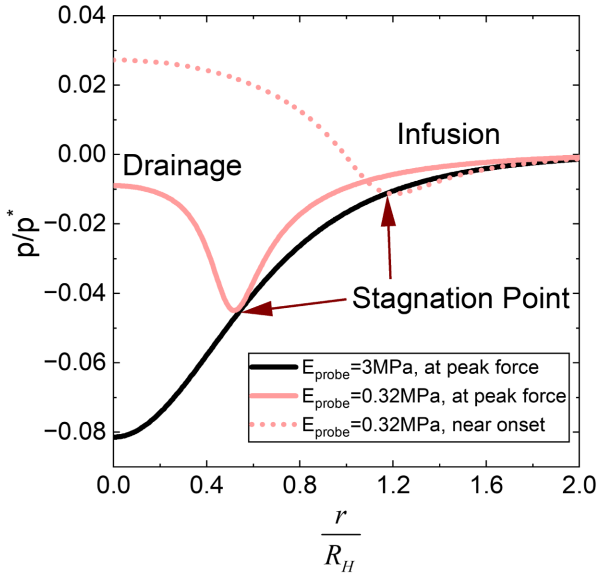

FIG. 5. Dimensionless pressure ($p^* = \eta v R/b^2$) vs dimensionless radial position ($R_H = \sqrt{2Rb}$) obtained from modeling the detachment of soft ($E_{\text{probe}} = 0.32$ MPa) and stiff ($E_{\text{probe}} = 3$ MPa) PDMS probes of $R = 6$ mm at 50 μm/s and $\eta = 1000$ Pa s, $b = 20$ μm. Retraction of the soft probe leads to lower fluid pressure and appearance of stagnation point delineating drainage and infusion regions.

from a rigid probe. Moreover, deformation of the soft probe leads to a negative pressure gradient at the center point, causing the fluid *drainage* from the center during detachment, while further away from the center, the pressure drop is positive, leading to the expected fluid *infusion*. Between the drainage and infusion regions, there is a stagnation point where the pressure gradient is zero. The stagnation point moves toward the center of the probe during retraction (Fig. 5). Because of incompressibility, the surfaces initially move closer at the center point during detachment. The combination of lower pressure and a stagnation point could suppress the Saffman-Taylor instabilities during the detachment from a soft probe; this will be the subject of future studies.

In summary, the detachment of a viscoelastic adhesive from soft surfaces suppresses the onset of Saffman-Taylor instabilities. While elasticity has been shown previously to impact Saffman-Taylor instabilities, we show here the connection with adhesion. Controlling the mode of failure during debonding between soft materials could impact adhesion (and pain) with skin. We attribute stabilization of the interface to elastohydrodynamic deformation of the probe caused by viscoelasticity. The elasticity parameter can serve as a guide for interfacial stability. A simple model shows that replacing a rigid probe with a soft one leads to a decrease in the pressure drop and the appearance of a stagnation point within the film, and both could lead to interface stabilization. Further studies are necessary to better understand the detachment process between two soft materials and the stabilization of the interface.

This work was supported by 3M and by the National Science Foundation (NSF-CMMI 1728082). Y. W. also acknowledges support from the National Natural Science Foundation of China (Grant No. 51804319).

*Corresponding author: jfrechette@berkeley.edu

[1] T. T. Al-Housseiny, P. A. Tsai, and H. A. Stone, Control of interfacial instabilities using flow geometry, Nat. Phys. **8**, 747 (2012).
[2] T. T. Al-Housseiny and H. A. Stone, Controlling viscous fingering in tapered hele-shaw cells, Phys. Fluids **25**, 092102 (2013).
[3] R. Arun, S. T. M. Dawson, P. J. Schmid, A. Laskari, and B. J. McKeon, Control of instability by injection rate oscillations in a radial Hele-Shaw cell, Phys. Rev. Fluids **5**, 123902 (2020).
[4] T. H. Beeson-Jones and A. W. Woods, On the selection of viscosity to suppress the Saffman–Taylor instability in a radially spreading annulus, J. Fluid Mech. **782**, 127 (2015).
[5] E. O. Dias and J. A. Miranda, Control of radial fingering patterns: A weakly nonlinear approach, Phys. Rev. E **81**, 016312 (2010).
[6] E. O. Dias, F. Parisio, and J. A. Miranda, Suppression of viscous fluid fingering: A piecewise-constant injection process, Phys. Rev. E **82**, 067301 (2010).
[7] T. Gao, M. Mirzadeh, P. Bai, K. M. Conforti, and M. Z. Bazant, Active control of viscous fingering using electric fields, Nat. Commun. **10**, 4002 (2019).
[8] H. Ma and Q. Yuan, Control of viscous fingering: From the perspective of energy evolution, Phys. Rev. Fluids **6**, 023901 (2021).
[9] M. Mirzadeh and M. Z. Bazant, Electrokinetic Control of Viscous Fingering, Phys. Rev. Lett. **119**, 174501 (2017).
[10] D. Pihler-Puzović, P. Illien, M. Heil, and A. Juel, Suppression of Complex Fingerlike Patterns at the Interface between Air and a Viscous Fluid by Elastic Membranes, Phys. Rev. Lett. **108**, 074502 (2012).
[11] H. S. Rabbani, D. Or, Y. Liu, C. Y. Lai, N. B. Lu, S. S. Datta, H. A. Stone, and N. Shokri, Suppressing viscous fingering in structured porous media, Proc. Natl. Acad. Sci. U.S.A. **115**, 4833 (2018).
[12] Z. Li, H. Zhang, X. Sun, and Y. Yang, Mitigating interfacial instability in polymer electrolyte-based solid-state lithium metal batteries with 4 V cathodes, ACS Energy Lett. **5**, 3244 (2020).
[13] W. Xu, J. Wang, F. Ding, X. Chen, E. Nasybulin, Y. Zhang, and J. G. Zhang, Lithium metal anodes for rechargeable batteries, Energy Environ. Sci. **7**, 513 (2014).
[14] S. B. Gorell and G. Homsy, A theory of the optimal policy of oil recovery by secondary displacement processes, SIAM J. Appl. Math. **43**, 79 (1983).
[15] T. M. Paronyan, E. M. Pigos, G. Chen, and A. R. Harutyunyan, Formation of ripples in graphene as a result of interfacial instabilities, ACS Nano **5**, 9619 (2011).
[16] R. Booth, On the growth of the mixing zone in miscible viscous fingering, J. Fluid Mech. **655**, 527 (2010).

[17] B. Jha, L. Cueto-Felgueroso, and R. Juanes, Fluid Mixing from Viscous Fingering, Phys. Rev. Lett. **106**, 194502 (2011).
[18] J. Marthelot, E. Strong, P. M. Reis, and P. T. Brun, Designing soft materials with interfacial instabilities in liquid films, Nat. Commun. **9**, 4477 (2018).
[19] S. Y. Heriot and R. A. Jones, An interfacial instability in a transient wetting layer leads to lateral phase separation in thin spin-cast polymer-blend films, Nat. Mater. **4**, 782 (2005).
[20] S. Liu, R. Deng, W. Li, and J. Zhu, Polymer microparticles with controllable surface textures generated through interfacial instabilities of emulsion droplets, Adv. Funct. Mater. **22**, 1692 (2012).
[21] M. B. Amar and D. Bonn, Fingering instabilities in adhesive failure, Physica (Amsterdam) **209D**, 1 (2005).
[22] S. Mora and M. Manna, Saffman-Taylor instability of viscoelastic fluids: From viscous fingering to elastic fractures, Phys. Rev. E **81**, 026305 (2010).
[23] S. Mora and M. Manna, From viscous fingering to elastic instabilities, J. Non-Newtonian Fluid Mech. **173**, 30 (2012).
[24] J. Nase, D. Derks, and A. Lindner, Dynamic evolution of fingering patterns in a lifted Hele–Shaw cell, Phys. Fluids **23**, 123101 (2011).
[25] P. G. Saffman and G. Taylor, The penetration of a fluid into a porous medium or Hele-Shaw cell containing a more viscous liquid, Proc. R. Soc. A **245**, 312 (1958).
[26] G. Bongrand and P. A. Tsai, Manipulation of viscous fingering in a radially tapered cell geometry, Phys. Rev. E **97**, 061101(R) (2018).
[27] T. T. Al-Housseiny, I. C. Christov, and H. A. Stone, Two-Phase Fluid Displacement and Interfacial Instabilities under Elastic Membranes, Phys. Rev. Lett. **111**, 034502 (2013).
[28] J. Nase, A. Lindner, and C. Creton, Pattern Formation During Deformation of a Confined Viscoelastic Layer: From a Viscous Liquid to a Soft Elastic Solid, Phys. Rev. Lett. **101**, 074503 (2008).
[29] P. H. A. Anjos, E. O. Dias, L. Dias, and J. A. Miranda, Adhesion force in fluids: Effects of fingering, wetting, and viscous normal stresses, Phys. Rev. E **91**, 013003 (2015).
[30] A. Lindner, D. Derks, and M. Shelley, Stretch flow of thin layers of Newtonian liquids: Fingering patterns and lifting forces, Phys. Fluids **17**, 072107 (2005).
[31] See Supplemental Material at http://link.aps.org/supplemental/10.1103/PhysRevLett.131.138201 for details on experimental protocols, model description, and material characterization, which includes Refs. [32–42].
[32] S. Ekgasit, N. Kaewmanee, P. Jangtawee, C. Thammacharoen, and M. Donphoongpri, Elastomeric PDMS planoconvex lenses fabricated by a confined sessile drop technique, ACS Appl. Mater. Interfaces **8**, 20474 (2016).
[33] J. N. Lee, C. Park, and G. M. Whitesides, Solvent compatibility of poly (dimethylsiloxane)-based microfluidic devices, Anal. Chem. **75**, 6544 (2003).
[34] J. D. Glover, C. E. McLaughlin, M. K. McFarland, and J. T. Pham, Extracting uncrosslinked material from low modulus sylgard 184 and the effect on mechanical properties, J. Polym. Sci. **58**, 343 (2020).
[35] Z. Cai, A. Skabeev, S. Morozova, and J. T. Pham, Fluid separation and network deformation in wetting of soft and swollen surfaces, Commun. Mater. **2**, 21 (2021).
[36] P. Karnal, P. Roberts, S. Gryska, C. King, C. Barrios, and J. Frechette, Importance of substrate functionality on the adhesion and debonding of a pressure-sensitive adhesive under water, ACS Appl. Mater. Interfaces **9**, 42344 (2017).
[37] K. L. Johnson, K. Kendall, and A. D. Roberts, Surface energy and the contact of elastic solids, Proc. R. Soc. A **324**, 301 (1971).
[38] J. N. Israelachvili, *Intermolecular and Surface Forces* (Academic Press, New York, 2015).
[39] Y. G. Kim, N. Lim, J. Kim, C. Kim, J. Lee, and K. H. Kwon, Study on the surface energy characteristics of polydimethylsiloxane (PDMS) films modified by C4F8/O2/Ar plasma treatment, Appl. Surf. Sci. **477**, 198 (2019).
[40] X. Xu, A. Jagota, D. Paretkar, and C. Y. Hui, Surface tension measurement from the indentation of clamped thin films, Soft Matter **12**, 5121 (2016).
[41] K. Mader-Arndt, Z. Kutelova, R. Fuchs, J. Meyer, T. Staedler, W. Hintz, and J. Tomas, Single particle contact versus particle packing behavior: Model based analysis of chemically modified glass particles, Granular Matter **16**, 359 (2014).
[42] K. L. Johnson, *Contact Mechanics* (Cambridge University Press, Cambridge, England, 1987).
[43] S. H. Jeong, S. Zhang, K. Hjort, J. Hilborn, and Z. Wu, PDMS-based elastomer tuned soft, stretchable, and sticky for epidermal electronics, Adv. Mater. **28**, 5830 (2016).
[44] Y. H. Ju, H. J. Lee, C. J. Han, C. R. Lee, Y. Kim, and J. W. Kim, Pressure-sensitive adhesive with controllable adhesion for fabrication of ultrathin soft devices, ACS Appl. Mater. Interfaces **12**, 40794 (2020).
[45] S. W. Kim, Y. H. Ju, S. Han, J. S. Kim, H. J. Lee, C. J. Han, C. R. Lee, S. B. Jung, Y. Kim, and J. W. Kim, A UV-responsive pressure sensitive adhesive for damage-free fabrication of an ultrathin imperceptible mechanical sensor with ultrahigh optical transparency, J. Mater. Chem. A **7**, 22588 (2019).
[46] Y. Liu, M. Pharr, and G. A. Salvatore, Lab-on-skin: A review of flexible and stretchable electronics for wearable health monitoring, ACS Nano **11**, 9614 (2017).
[47] H. Moon, K. Jeong, M. J. Kwak, S. Q. Choi, and S. G. Im, Solvent-free deposition of ultrathin copolymer films with tunable viscoelasticity for application to pressure-sensitive adhesives, ACS Appl. Mater. Interfaces **10**, 32668 (2018).
[48] E. M. Thomas, H. Fu, R. C. Hayward, and A. J. Crosby, Geometry-controlled instabilities for soft–soft adhesive interfaces, Soft Matter **18**, 8098 (2022).
[49] L. Afferrante and G. Carbone, The ultratough peeling of elastic tapes from viscoelastic substrates, J. Mech. Phys. Solids **96**, 223 (2016).
[50] H. Perrin, A. Eddi, S. Karpitschka, J. H. Snoeijer, and B. Andreotti, Peeling an elastic film from a soft viscoelastic adhesive: Experiments and scaling laws, Soft Matter **15**, 770 (2019).
[51] E. Pierro, L. Afferrante, and G. Carbone, On the peeling of elastic tapes from viscoelastic substrates: Designing materials for ultratough peeling, Tribol. Int. **146**, 106060 (2020).

[52] R. H. Plaut, Peeling pressure-sensitive adhesive tape from thin elastic strip, J. Adhes. **86**, 675 (2010).
[53] R. H. Plaut, Two-dimensional analysis of peeling adhesive tape from human skin, J. Adhes. **86**, 1086 (2010).
[54] J. Renvoise, D. Burlot, G. Marin, and C. Derail, Peeling of PSAs on viscoelastic substrates: A failure criterion, J. Adhes. **83**, 403 (2007).
[55] Y. Sugizaki, T. Shiina, Y. Tanaka, and A. Suzuki, Effects of peel angle on peel force of adhesive tape from soft adherend, J. Adhes. Sci. Technol. **30**, 2637 (2016).
[56] T. Zhang, H. Yuk, S. Lin, G. A. Parada, and X. Zhao, Tough and tunable adhesion of hydrogels: Experiments and models, Acta Mech. **33**, 543 (2017).
[57] P. Roberts, G. A. Pilkington, Y. Wang, and J. Frechette, A multifunctional force microscope for soft matter with *in situ* imaging, Rev. Sci. Instrum. **89**, 043902 (2018).
[58] P. Karnal, A. Jha, H. Wen, S. Gryska, C. Barrios, and J. Frechette, Contribution of surface energy to pH-dependent underwater adhesion of an acrylic pressure-sensitive adhesive, Langmuir **35**, 5151 (2019).
[59] A. Ghatak, M. K. Chaudhury, V. Shenoy, and A. Sharma, Meniscus Instability in a Thin Elastic Film, Phys. Rev. Lett. **85**, 4329 (2000).
[60] A. Ghatak and M. K. Chaudhury, Adhesion-induced instability patterns in thin confined elastic film, Langmuir **19**, 2621 (2003).
[61] M. K. Chaudhury, A. Chakrabarti, and A. Ghatak, Adhesion-induced instabilities and pattern formation in thin films of elastomers and gels, Eur. Phys. J. E **38**, 82 (2015).
[62] J. S. Biggins and L. Mahadevan, Meniscus instabilities in thin elastic layers, Soft Matter **14**, 7680 (2018).
[63] S. Yu and H. Jiang, Adhesion-induced instability regulates contact mechanics of soft thin elastic films, ACS Appl. Mater. Interfaces **13**, 21994 (2021).
[64] A. R. Mojdehi, D. P. Holmes, and D. A. Dillard, Revisiting the generalized scaling law for adhesion: Role of compliance and extension to progressive failure, Soft Matter **13**, 7529 (2017).
[65] M. D. Bartlett and A. J. Crosby, Scaling normal adhesion force capacity with a generalized parameter, Langmuir **29**, 11022 (2013).
[66] S. Yu and H. Jiang, Adhesion-induced instability regulates contact mechanics of soft thin elastic films, ACS Appl. Mater. Interfaces **13**, 21994 (2021).
[67] K. R. Shull, Contact mechanics and the adhesion of soft solids, Mater. Sci. Eng. R Rep. **36**, 1 (2002).
[68] C. Creton and M. Ciccotti, Fracture and adhesion of soft materials: A review, Rep. Prog. Phys. **79**, 046601 (2016).
[69] Y. Wang, C. Dhong, and J. Frechette, Out-of-Contact Elastohydrodynamic Deformation due to Lubrication Forces, Phys. Rev. Lett. **115**, 248302 (2015).
[70] R. H. Davis, J. M. Serayssol, and E. Hinch, The elastohydrodynamic collision of two spheres, J. Fluid Mech. **163**, 479 (1986).
[71] Z. Zhang, V. Bertin, M. Arshad, E. Raphael, T. Salez, and A. Maali, Direct Measurement of the Elastohydrodynamic Lift Force at the Nanoscale, Phys. Rev. Lett. **124**, 054502 (2020).
[72] M. H. Essink, A. Pandey, S. Karpitschka, C. H. Venner, and J. H. Snoeijer, Regimes of soft lubrication, J. Fluid Mech. **915** (2021).
[73] Y. Wang, Z. Feng, and J. Frechette, Dynamic adhesion due to fluid infusion, Curr. Opin. Colloid Interface Sci. **50**, 101397 (2020).
[74] Y. Wang, M. R. Tan, and J. Frechette, Elastic deformation of soft coatings due to lubrication forces, Soft Matter **13**, 6718 (2017).